X-ray Faraday effect at the $L_{2,3}$ edges of Fe, Co, and Ni: Theory and experiment

J. Kuneš* and P. M. Oppeneer
Institute of Solid State and Materials Research, P.O. Box 270016, D-01171 Dresden, Germany

H.-Ch. Mertins, F. Schäfers, A. Gaupp, and W. Gudat
BESSY GmbH, Albert-Einstein-Str. 15, D-12489 Berlin, Germany

P. Novák
Institute of Physics, Academy of Sciences, Cukrovarnická 10, CZ-162 53 Prague, Czech Republic
(Received 19 April 2001; published 11 October 2001)

The x-ray Faraday effect at the $L_{2,3}$ edges of the $3d$ ferromagnets Fe, Co, Ni and of $Fe_{0.5}Ni_{0.5}$ alloy is studied both theoretically and experimentally. We perform *ab initio* calculations of the x-ray Faraday effect on the basis of the local spin-density approximation and we adopt the linear-response formalism to describe the material's response to the incident light. Experimental x-ray Faraday rotation and ellipticity spectra are measured with linearly polarized soft-x-ray synchrotron radiation at BESSY, Berlin. The measured x-ray Faraday rotations are remarkably large, up to 2.8×10^5 deg/mm, which is more than one order of magnitude larger than those observed in the visible range. From the measured Faraday spectra we determine the intrinsic dichroic contributions to the dispersive and absorptive parts of the refractive index, and compare these to *ab initio* calculated counterparts. The theoretical dichroic spectra are in good qualitative agreement with the experimental data. The inclusion of the spin polarization of the core states leads to a small, yet non-negligible, improvement of the theoretical dichroic spectra. Our results illustrate that the many-particle x-ray excitation spectrum can be sufficiently well approximated by the Kohn-Sham single-particle spectrum. From the computed magneto-x-ray spectra we determine, using the sum rules, the orbital moments, which we compare to the exact orbital moments.

DOI: 10.1103/PhysRevB.64.174417 PACS number(s): 78.70.Dm, 78.20.Ls

I. INTRODUCTION

X-ray magneto-optical spectroscopies have developed rapidly over the last few years, during which they have become established as valuable tools for the investigation of magnetic properties of materials.[1–11] Among the various available magneto-x-ray spectroscopies there are commonly two distinctions made. The first distinction is with regard to the polarization state of the incident x-ray light being used, i.e., whether it is circularly or linearly polarized, and the second one is whether the intensity or the polarization of the light beam after its interaction with the magnetic material is measured. Most frequently applied are circularly polarized x rays, which are employed to measure the x-ray magnetic circular dichroism (XMCD). The XMCD has gained appreciable importance due to the sum rules,[12,13] which allow one to evaluate the spin and orbital moment of a specific element in the material from a spectral integral over the XMCD spectrum (see, e.g., Refs. 14–17). Less frequently applied are linearly polarized x rays, which are employed to measure the resonant magnetic x-ray scattering,[5] the x-ray magnetic linear dichroism (XMLD) (e.g., Refs. 18 and 19), and the x-ray Faraday effect (XFE).[4,7–10] The resonant magnetic x-ray scattering, the XMCD, and XMLD are intensity measurements, whereas the x-ray Faraday effect demands a polarization-state analysis. Both the Faraday rotation, which is the rotation of the polarization plane upon transmission, and the Faraday ellipticity, which is the amount by which the transmitted light has become elliptically polarized, are to be determined. While it is in itself already a complicated task to make a polarization analysis, this is even more so in the soft-x-ray energy region, where suitable analyzers are rare. So far only a few experimental studies of the XFE were reported.[4,7–11] The x-ray Faraday effect at the K edge of Co was investigated in Ref. 4. More recently, the Faraday effect at the $L_{2,3}$ edges of Fe (Ref. 7), of Pt in Fe_3Pt (Ref. 8), and of Fe, Co, and Ni (Refs. 9–11) were measured. These recent measurements have demonstrated that XFE experiments can be employed as an alternative to XMCD measurements for determining the dichroic spectra.[8,9] The advantages over the XMCD technique are that the dichroic part in both the absorptive and dispersive spectrum can be obtained from a single XFE measurement and the wider availability of x-ray sources for linearly polarized light.

In the recent XFE measurements performed by some of us, the full magneto-x-ray spectra at the L_2 ($2p_{1/2}$) and L_3 ($2p_{3/2}$) edges of Co, Fe, and Ni in $Fe_{0.5}Ni_{0.5}$ were obtained.[9] From these recent experiments and from new experiments to be presented here, we have obtained the complete dichroic spectra $\Delta\delta(\omega)$, $\Delta\beta(\omega)$, to the dispersive and absorptive parts of the refractive indices. The refractive indices can be written as $n_{\pm}=1-(\delta_0\pm\Delta\delta)+i(\beta_0\pm\Delta\beta)$, which is valid for the so-called polar geometry where the magnetization and propagation direction of the light are parallel. The incident linearly polarized light is decomposed into two circularly polarized waves of opposite helicity. The indices $\pm$ refer to the parallel or antiparallel orientation of photon helicity and magnetization, and the δ_0 (β_0) stands for the dispersive (absorptive) component, of the unmagnetized material. $\Delta\beta$ and $\Delta\delta$ are the intrinsic material's magnetic

quantities, which comprise information on the resonant transitions from the $2p_{1/2}$ and $2p_{3/2}$ core states to the empty spin-polarized d states, and therefore are highly relevant to the $3d$ ferromagnetism of Fe, Co, and Ni.

Concurrent to our XFE experiments, we have performed *ab initio* calculations of the magneto-x-ray effects. Previously, several calculations of the XMCD, but also of the XFE were reported.[20–26] However, since precise XFE data at the $L_{2,3}$ edges of Fe, Co, and Ni, were not available, a fully conclusive comparison with experiment could not be made. This comparison is one of the goals of the present paper. The calculations, ours as well as previous, are based on the density-functional theory in the local spin-density approximation (LSDA).[27] This implies that the many-body quasiparticle excitation spectrum is approximated by the Kohn-Sham single-particle spectrum. We apply furthermore the Kubo linear-response theory for evaluating the material's response to the incident x-ray beam. As we shall show, the *ab initio* calculations provide a good description of the experimental dichroic x-ray spectra. Consequently, the XFE and related magneto-x-ray effects can be investigated theoretically on the basis of first-principles calculations. Previously, very little attention was devoted to the influence that the exchange splitting of the $2p$ core states has on the XFE spectra. We find that taking the exchange splitting of the core states into account does improve the agreement between the *ab initio* calculated and measured dichroic spectra $\Delta\delta$, $\Delta\beta$. Furthermore, using the sum rules, we determine from the calculated magneto-x-ray spectra the spin and orbital moments, which we compare to directly calculated moments.

In the following section we first describe schematically the experimental technique. Expressions for the XFE in the experimental geometry are derived in Sec. III, and in Sec. IV we outline the computational scheme. Results and conclusions are presented in the Secs. V and VI.

II. EXPERIMENTAL SETUP

The magneto-x-ray experiments were performed at the Berlin synchrotron radiation source BESSY I using the plane grating Petersen-type (SX700) monochromator[28] PM3 and at BESSY II using the elliptical undulator UE56-PGM,[29] with spectral resolution $E/\Delta E=700$ and $E/\Delta E=2500$, respectively. Our samples consisted of 50-nm-thick amorphous films that were either magnetron-sputter deposited on 100 nm Si_3N_4 foils (Fe, Co) or electron-beam evaporated on 1 μm Mylar ($Fe_{0.5}Ni_{0.5}$). Our experimental setup is shown schematically in Fig. 1. The transmission sample can be placed at any incident angle ϕ_i between 90° (grazing) and 0° (normal incidence). The polarization of the incident x-ray beam was in the plane of incidence. A magnetic coil system supplies variable magnetic fields of -500 Oe$\leqslant H\leqslant +500$ Oe lying in the sample's plane and in the plane of incidence; i.e., the measurements were carried out in the longitudinal geometry. In the visible spectral range Faraday effect measurements are normally performed in the polar geometry, where the magnetization is perpendicular to the films. We chose the longitudinal geometry to assure that all measurements could be performed with magnetically saturated films. The linear polarization analysis was performed by rotating a W/B_4C reflection multilayer (300 periods, period 1.2 nm, angle of incidence close to the Brewster angle) around the beam by the angle α (analyzer scan) while recording the transmitted intensity.[30] The experiment is described in detail in Ref. 9.

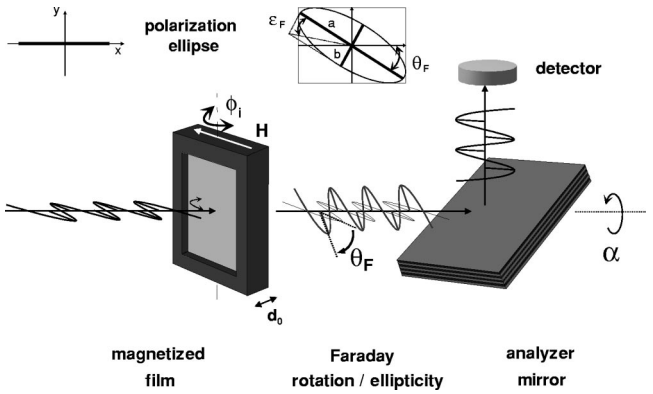

FIG. 1. Schematic setup for Faraday measurements on magnetic films with angle of incidence ϕ_i and magnetic field **H**. The Faraday rotation angle θ_F and Faraday ellipticity ε_F are detected by an azimuthal rotation of the analyzer and detector around the beam. The rotation θ_F and ellipticity ε_F of the transmitted light are indicated in the polarization ellipse with main axes a and b, where $\tan\varepsilon_F=b/a$.

III. FORMULAS FOR X-RAY MO EFFECTS

Expressions for magneto-x-ray effects can be derived from the Fresnel equation for the magnetic refractive indices of the material and the continuity requirements for electromagnetic fields at the interface. These expressions depend on both the magnetization direction and the propagation direction of the beam. The simplest configuration for which exact expressions for MO effects can be derived is the polar geometry where the magnetization and incident light are normal at the material's surface. The electric field eigenmodes in the material are left- and right-circularly polarized waves, which would each match continuously to an incident circularly polarized beam. The incident linearly polarized x-ray beam can be written as the sum of equal amounts of left- and right-circularly polarized light. The Faraday rotation θ_F and the Faraday ellipticity ε_F can be related to the refractive indices $n_\pm$ for left- and right-circularly polarized light by the exact equation[31]

$$\left(\frac{1-\tan\varepsilon_F}{1+\tan\varepsilon_F}\right)e^{2i\theta_F}=e^{i\omega d_t(n_+-n_-)/c}, \tag{1}$$

where d_t is the transmitted thickness of the sample, $d_t=d_0$ at normal incidence. The influence of the magnetization on the index of refraction is given by the difference of n_+ and n_-, which is normally small. From the Fresnel equation one obtains for $n_\pm$ in the present geometry

$$n_\pm^2=\epsilon_{xx}\pm i\epsilon_{xy}, \tag{2}$$

where ϵ_{xx} and ϵ_{xy} and are the diagonal and off-diagonal elements, respectively, of the permittivity tensor. Since MO effects are small compared to the nonmagnetic response, Eq. (1) can be expanded to first order in the small quantities, which gives

$$\theta_F + i \tan \varepsilon_F \approx \frac{\omega d_0}{2c}(n_+ - n_-) \approx \frac{\omega d_0}{2c} \frac{i\epsilon_{xy}}{\epsilon_{xx}^{1/2}}. \tag{3}$$

The off-diagonal permittivity ϵ_{xy} is the magnetically active component, which is antisymmetric in the magnetization: $\epsilon_{xy}(-\boldsymbol{M}) = -\epsilon_{xy}(\boldsymbol{M})$.

In the case that the incoming light is not normal, but oblique at an incident angle ϕ_i (see Fig. 1), it becomes rather complicated to derive exact expressions for the MO quantities. However, it is always possible to give approximate equations to lowest order in the small quantities. At oblique incidence the actual transmitted thickness d_t of the sample depends on the refraction angle ϕ_t, i.e., $d_t = d_0/\cos\phi_t$. In the longitudinal geometry at oblique incidence one can measure the Faraday effect provided the magnetization has a nonzero component parallel to the propagation direction of the beam. The approximate solutions to the Fresnel equation are in this geometry,[32] to first order in ϵ_{xy},

$$n_\pm^2 \approx \epsilon_{xx} \pm i\epsilon_{xy} \sin\phi_t^\pm, \tag{4}$$

where $\phi_t^\pm$ are the refraction angles of the two eigenmodes. To first order in ϵ_{xy} one can replace $\phi_t^\pm$ by ϕ_t in Eq. (4), where ϕ_t is the angle of refraction of the nonmagnetized material. It can be shown that the approximate expression for the Faraday effect in this case becomes[31]

$$\theta_F + i \tan \varepsilon_F \approx \frac{\omega d_0}{2c} \frac{i\epsilon_{xy} \sin\phi_t^\pm}{\epsilon_{xx}^{1/2} \cos\phi_t} \approx \frac{\omega d_0}{2c} \frac{i\epsilon_{xy}}{\epsilon_{xx}^{1/2}} \tan\phi_t. \tag{5}$$

Here $\tan\phi_t$ can be rewritten further using Snell's law. For x-ray light one may replace $\tan\phi_t \approx \tan\phi_i$ to a good approximation. From this expression it is obvious that potentially a large Faraday rotation can be achieved from an in-plane magnetized material for a large ϕ_t of 70° or more, i.e., at grazing incidence, as was indeed observed experimentally.[9]

As written in the Introduction, the intrinsic dichroic material's quantities of interest are $\Delta\delta$ and $\Delta\beta$. From Eq. (5) it is evident that these quantities can readily be obtained from the measured quantities θ_F, ε_F, in the longitudinal geometry through

$$\theta_F = -\frac{\omega d_0}{c} \Delta\delta \tan\phi_t, \quad \tan\varepsilon_F = \frac{\omega d_0}{c} \Delta\beta \tan\phi_t. \tag{6}$$

The XFE is measured with linearly polarized x rays, but a similar magneto-optical quantity can be measured with circularly polarized light as well. In XMCD experiments one measures the dichroism, which is given by the asymmetry parameter A and defined as

$$A = (T_+ - T_-)/(T_+ + T_-), \tag{7}$$

where $T_\pm$ are the transmission coefficients of left- and right-handed circularly polarized x rays. It can be shown that the XMCD asymmetry parameter is directly proportional to the Faraday ellipticity (see Refs. 8, 9, and 33). In XMCD experiments, however, one measures only one of the dichroic quantities ($\Delta\beta$), while the other one has to be derived from a Kramers-Kronig transformation. In XFE experiments, on the other hand, one measures *both* dichroic quantities $\Delta\beta$, $\Delta\delta$ in a single experiment. However, at present the XMCD can be measured more precisely than the Faraday ellipticity.

Magneto-optical effects can also be measured in the reflection of linearly polarized x rays off a magnetized material, in which case the effect is called the magneto-optical Kerr effect (MOKE). Both in the longitudinal and polar configuration the detection of MOKE requires a polarization-state analysis. So far no MOKE spectra have been measured in the x-ray energy range, but the existence of the x-ray MOKE could be proved at a single soft-x-ray frequency.[7,34] Although experimental spectra for the x-ray MOKE are therefore not yet available, theoretical predictions can already be made for the purpose of comparison with future experiments. In the polar geometry at normal incidence the Kerr rotation θ_K and Kerr ellipticity ε_K are given by the (exact) expression[31]

$$\left(\frac{1-\tan\varepsilon_K}{1+\tan\varepsilon_K}\right) e^{2i\theta_K} = \frac{1+n_-}{1-n_-} \frac{1-n_+}{1+n_+}. \tag{8}$$

This expression can be approximated again for small θ_K, ε_K, and $n_+ - n_-$, and, similar to the XFE [Eq. (3)], it can be formulated in terms of ϵ_{xy} and ϵ_{xx}.

The above expressions exemplify that the theory of magneto-x-ray effects can be developed on the basis of a single quantity, the permittivity tensor. As the permittivity and conductivity tensor $\sigma_{\alpha\beta}$ are related through $\epsilon_{\alpha\beta} = \delta_{\alpha\beta} + 4\pi i \sigma_{\alpha\beta}/\omega$, one may equivalently compute the conductivity tensor. Its evaluation from first principles is the prime task to be performed, which is outlined in the following.

IV. COMPUTATIONAL METHOD

A. Calculation of the permittivity tensor

The near-edge x-ray and magneto-x-ray effects originate from excitations of the core electrons to unoccupied valence states close above the Fermi level. The response of the solid to an external electromagnetic field is to linear order in the field described by the dielectric or conductivity tensor, each of which is sufficient to describe all experimentally accessible quantities. We start from the Kubo linear-response expression for $\sigma_{\alpha\beta}$ in a single-particle formulation (see, e.g., Ref. 31), in the limit of zero lifetime broadening, which we rewrite in several steps. First, the occurring current operator matrix elements containing the relativistic impulse operator are replaced by the matrix elements of the nonrelativistic impulse operator, $\boldsymbol{p} = -i\hbar\boldsymbol{\nabla}$, which holds to a very good approximation.[35] Second, we use the fact that the core states are localized and therefore the impulse matrix elements can be replaced by dipolar moment matrix elements. The result-

ing expressions for the absorptive parts of the permittivity components, i.e., $\mathrm{Im}\,\epsilon_{xx}=\epsilon_{xx}^{(2)}$, $\mathrm{Re}\,\epsilon_{xy}=\epsilon_{xy}^{(1)}$, are

$$\epsilon_{xx}^{(2)}(\omega)=\frac{4\pi^2e^2}{\hbar V_{uc}}\mathrm{Re}\sum_{\boldsymbol{k}}\sum_{\substack{c\ \mathrm{occ.}\\ n\ \mathrm{un.}}} r_{nc}^{x}(\boldsymbol{k})r_{cn}^{x}(\boldsymbol{k})\,\delta(\omega-\omega_{nc}(\boldsymbol{k})),$$

$$\epsilon_{xy}^{(1)}(\omega)=\frac{4\pi^2e^2}{\hbar V_{uc}}\mathrm{Im}\sum_{\boldsymbol{k}}\sum_{\substack{c\ \mathrm{occ.}\\ n\ \mathrm{un.}}} r_{nc}^{x}(\boldsymbol{k})r_{cn}^{y}(\boldsymbol{k})\,\delta(\omega-\omega_{nc}(\boldsymbol{k})), \tag{9}$$

where c labels the core states and $n,\boldsymbol{k}$ the unoccupied valence-band states, $\hbar\omega_{nc}(\boldsymbol{k})\equiv\epsilon_{n\boldsymbol{k}}-\epsilon_c$, the energy difference between the core and valence states, V_{uc} is the unit cell volume, and the $r_{nc}^{x,y}(\boldsymbol{k})$ are the dipolar matrix elements. The positions x, y, refer to the coordinate system centered at the atom of interest. In a practical evaluation of the full permittivity tensor, first a convolution with a Lorentzian to account for lifetime broadening and subsequently a Kramers-Kronig transformation are performed to obtain the dispersive parts. The dipolar matrix elements can be rewritten in terms of p-type spherical harmonics Y_{1m}. A nice feature of Eq. (9) is that the transition energy, which can be obtained only approximately within a one-particle formulation, enters only the δ function and can therefore easily be renormalized as to coincide with the experimental edge energy.

In the present numerical implementation of Eq. (9) we use the full-potential, linearized augmented plane-wave method (FLAPW) method as implemented in the WIEN97 code.[36] The wave functions are expanded into products of spherical harmonics Y_{lm} and radial wave functions within a given atomic sphere. When we neglect the effect of the exchange field on the core states, then these can be expressed as products of radial solutions of the Kohn-Sham-Dirac equation and angular functions having the relativistic symmetry. Furthermore, we adopt a spherical approximation for the core potential. The relativistic valence states are computed within the full, nonspherical potential, using the second variational approach to self-consistently include the spin-orbit interaction.[37] Among the valence states there are three kinds of radial functions that are used for the expansion at a given orbital quantum number. These are the initial solutions of the scalar-relativistic approximation to the Kohn-Sham-Dirac equation in a spherical potential at a given expansion energy, its energy derivative, and optionally local orbitals that could be included as well in the basis.[38] The dipolar matrix elements in the FLAPW basis read

$$\begin{aligned}\langle\psi_c(l_c,j,j_z)|rY_{1\mu}|\psi_{n\boldsymbol{k}}\rangle=&\sum_{l,m,s,m_c}\{a_{lm}^{s}(\boldsymbol{k})A_{lj}^{s}+b_{lm}^{s}(\boldsymbol{k})B_{lj}^{s}\\&+c_{lm}^{s}(\boldsymbol{k})C_{lj}^{s}\}\\&\times(l_c,m_c,\tfrac{1}{2},s|l_c,\tfrac{1}{2},j,j_z)\\&\times\langle Y_{l_cm_c}|Y_{1\mu}Y_{lm}\rangle.\end{aligned} \tag{10}$$

Here a_{lm}^{s}, b_{lm}^{s}, and c_{lm}^{s} are the expansion coefficients of the wave function inside a given atomic sphere with radius R_{MT} corresponding to the three types of radial functions used within the FLAPW method. The spherical harmonics indices l and m correspond to the quantum numbers of the orbital expansion of the valence states, and m_c to the expansion of a core state, and s is the spin quantum number. The core states are identified by the orbital quantum number l_c and relativistic quantum numbers j, j_z. The radial integrals A_{lj}^{s} are defined by

$$A_{lj}^{s}=\int_0^{R_{MT}}R_l^{s}(r)R_{l_cj}^{c}(r)r^3dr; \tag{11}$$

i.e., the integral is taken between the valences-state radial functions R_l^{s} and the core radial function $R_{l_cj}^{c}$. The B_{lj}^{s} and C_{lj}^{s} are given by equivalent expressions, but for the other two kinds of radial valence functions. The $(l_c,m_c,\frac{1}{2},s|l_c,\frac{1}{2},j,j_z)$ are vector-coupling coefficients. The angular integrals of three spherical harmonics $\langle Y_{l_cm_c}|Y_{1\mu}Y_{lm}\rangle$ are the standard Gaunt coefficients. Due to the symmetry properties of the spherical harmonics, which result in the so-called selection rules, the summations in Eq. (10) reduce to $l=l_c\pm1$, $m=m_c-1,0,+1$, and to a single summation over the spin variable. The latter summation reduction comes about because we restrict ourselves in the present approach to the nonrelativistic dipolar approximation for the impulse operator.

In our computational scheme we pay attention to the role of the exchange splitting of the core levels. We employ first-order perturbation theory to account for the spin splitting of the core states. In particular, we solve the Dirac equation with the averaged potential $\frac{1}{2}[V_{\uparrow}(\mathbf{r})+V_{\downarrow}(\mathbf{r})]$ and treat the term $\Delta=\frac{1}{2}[V_{\uparrow}(\mathbf{r})-V_{\downarrow}(\mathbf{r})]\sigma_z$ (where the quantization local z axis was chosen along the net-magnetization direction) as a perturbation. Neglecting the hybridization between the states of different total momentum and using the fact that the matrix elements of Δ between states of different magnetic quantum number j_z are zero, we obtain a first-order shift of the eigenenergies, whereby the energy degeneracy of the core states is removed.

B. Details of the calculation

Self-consistent band-structure calculations were performed for bcc Fe, hcp and fcc Co, fcc Ni, and an $Fe_{0.5}Ni_{0.5}$ alloy. For all these materials the exchange field was constrained to the [001] direction. The number of k points in the irreducible wedge of the Brillouin zone, used in the calculation of the components of the dielectric tensor, exceeded 500. The LSDA exchange-correlation potential of Perdew and Wang[39] was adopted. The present implementation of the FLAPW method[36] uses the spin-orbit coupling for the valence states included self-consistently in the second variational step. For a detailed description of the implementation of the spin-orbit coupling we refer to Ref. 37.

V. RESULTS

A. X-ray Faraday effect of Fe, Co, and Ni

Using the above given approach, we calculated *ab initio* the components of the dielectric tensors of bcc Fe, hcp Co,

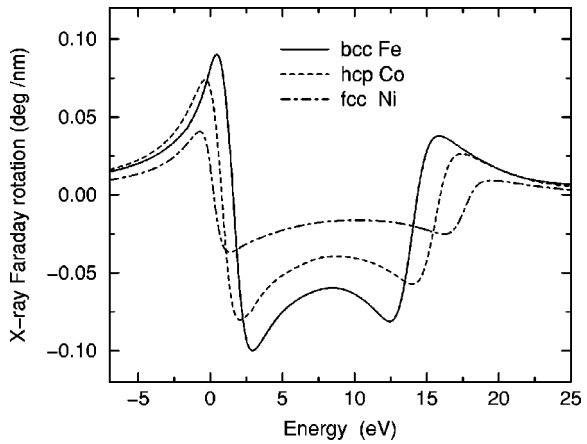

FIG. 2. *Ab initio* calculated polar x-ray Faraday rotations at the L edges of bcc Fe, hcp Co, and fcc Ni.

and fcc Ni, from which we computed their polar x-ray Faraday rotations. These are shown in Fig. 2. The depicted Faraday rotations were all computed with the spin polarization of the core states included. We mention that since the magnitude of the studied magneto-x-ray effects is expected to be much larger than their counterparts in the visible region, we used exact expressions instead of the approximate ones commonly employed in the visible region (cf. Ref. 31). To account for the experimental resolution and the lifetime broadening, a Lorentzian spectral broadening of 0.9 and 1.4 eV was applied at the L_3 and L_2 edges, respectively.[40] The features of the x-ray Faraday rotations can be understood qualitatively: The overall width of the spectra is determined by the spin-orbit splitting of the $2p_{1/2}$ and $2p_{3/2}$ states. This splitting is the largest for Ni and smallest for Fe. The magnitude of the x-ray Faraday rotation, on the other hand, basically follows the amount of spin polarization of the $3d$ valence states. This quantity is the largest for Fe and the smallest for Ni, and, likewise, the calculated Faraday rotation is the largest for Fe. In Fig. 2 we have shifted the respective positions of the absorption edges to coincide with one another. Note that the polar x-ray Faraday rotations at the $L_{2,3}$ edges are an order of magnitude larger than the polar Faraday rotations measured in the visible energy range.[41] Our measurements of the x-ray Faraday rotations[9] performed in the longitudinal geometry yielded also values much larger than those known from the visible range.

B. Intrinsic dichroic quantities

From the measured longitudinal XFE spectra we have determined the intrinsic dichroic parts $\Delta\beta$ and $\Delta\delta$ of the refractive indices. Since the XFE experiments were performed on a thin film of amorphous Co and of $Fe_{0.5}Ni_{0.5}$ alloy, we have calculated the dichroic quantities for fcc Co and for an ordered $Fe_{0.5}Ni_{0.5}$ alloy derived from bcc Fe by replacing the central atom with Ni. These systems were chosen in order to mimic optimally the experimental materials. In the ordered $Fe_{0.5}Ni_{0.5}$ alloy the average nearest-neighbor distance of fcc Ni and of bcc Fe was used for the Fe-Ni separation.

The calculated and experimental dichroic spectra at the L edge of Fe in $Fe_{0.5}Ni_{0.5}$ are shown in Fig. 3. The quantities

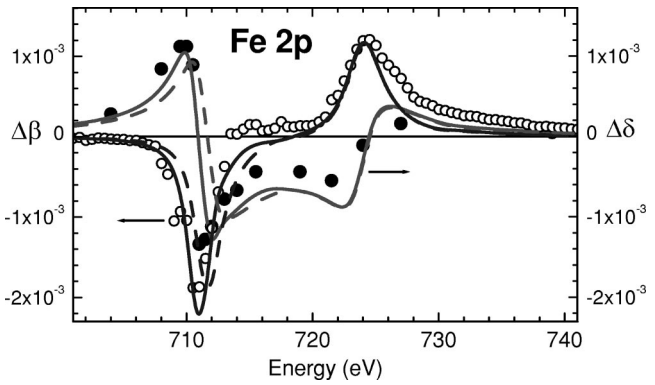

FIG. 3. Experimental and calculated dichroic spectra $\Delta\beta$ and $\Delta\delta$ at the L edge of Fe in $Fe_{0.5}Ni_{0.5}$. The two calculated spectra illustrate the influence of the exchange splitting of the $2p$ core states on the dichroic spectra. The dashed curves give the dichroic spectra computed without exchange splitting of the core states.

have been scaled by a factor of 2, because iron only constitutes half of the sample thickness. It is immediately seen that there exists a very good agreement between experiment and theory. The two theoretical curves correspond to calculations either with (solid curves) or without (dashed curves) including the spin splitting of the $2p$ core states. The calculation which takes the $2p$ cores splitting into account reproduces the measured spectra better. In particular at the L_3 edge the core polarization induces a shift of 1 eV in the $\Delta\beta$ spectrum to lower energies, which yields a better correspondence to the experiment. The L_2 edge is not affected. A similar shift occurs in the $\Delta\delta$ spectrum at the L_3 edge, where the measured data points at 710–712 eV are better reproduced by the calculation which includes the core polarization. The reason for the influence of the core polarization is explained in detail below. We remark that the measured dichroic spectra of Fe in $Fe_{0.5}Ni_{0.5}$ can be reasonably well approximated by $\Delta\beta$, $\Delta\delta$ spectra computed for pure Fe, because these spectra are dominated by the resonant $2p$ to $3d$ optical transitions.

Figure 4 shows the corresponding dichroic spectra for Co. Particularly the experimental and calculated $\Delta\beta$ spectra agree very well. While the shape of the experimental di-

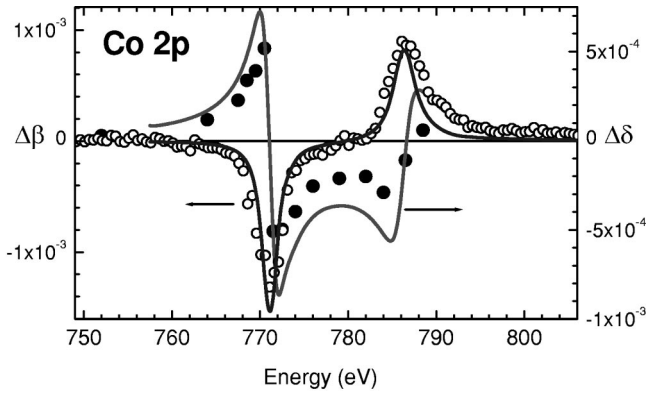

FIG. 4. As Fig. 3, but for the L edge of Co. The experimental dichroic spectra were measured for amorphous Co, and the calculated spectra were obtained for fcc Co.

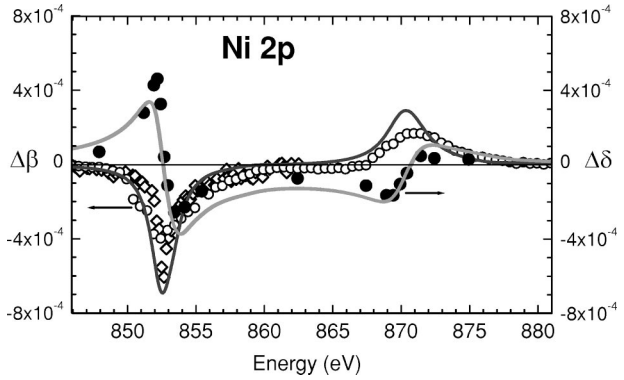

FIG. 5. As Fig. 3, but for the L edge of Ni in $Fe_{0.5}Ni_{0.5}$. The experimental $\Delta\beta$ data points were measured with two different spectral resolutions: $E/\Delta E=700$ (○) and $E/\Delta E=2500$ (◇).

chroic $\Delta\delta$ spectrum is well reproduced by the *ab initio* calculation, its measured magnitude is smaller in the region between the L_2 and L_3 edges. At the moment we have no explanation for the magnitude difference, but we suspect that it arises from the measurement technique (see also Ref. 11). A second difference between theoretical and measured spectra is recognizable in the $\Delta\beta$ spectrum at the high-energy side of the L_2 edge, where the theoretical curve falls off steeper than the experiment. This also happens for Fe (see Fig. 3). The overall correspondence between theory and experiment is none the less very good.

The calculated and experimental dichroic spectra at the Ni L edge of Ni in $Fe_{0.5}Ni_{0.5}$ alloy are shown in Fig. 5. Once again, the experimental and theoretical spectra compare satisfactorily. There are two experimental results given for the $\Delta\beta$ spectrum of Ni. One $\Delta\beta$ spectrum was measured with a lower energy resolution (at BESSY I, ○ in Fig. 5) than that of the other measurements, which explains why this $\Delta\beta$ curve is smoother and less peaked. The other $\Delta\beta$ data points (◇) were measured at the L_3 edge with the higher spectral resolution of BESSY II. It could be that the measured $\Delta\beta$ spectra contain a weak shoulder at 855 eV. It could be that the measured $\Delta\beta$ spectrum contains a weak shoulder at 855 eV. Previously a weak shoulder (labeled B) was observed in the XMCD spectrum of Ni at this energy.[42,43] The origin of this weak shoulder is not understood, but it could be a many-particle excitation feature. This interpretation is corroborated by the absence of such shoulder in the calculated single-particle spectrum. Nonetheless, our whole set of results emphasizes that the full x-ray Faraday spectra of transition metals can be quite well described by the single-particle Kohn-Sham approach. Although previously calculations of the XFE were reported,[21,22,24,25] the agreement to the available experimental data could not be considered as such good. Our new measurements of the XFE provide accurate dichroic spectra, which are highly suited for a conclusive comparison to first-principles theoretical spectra.

C. Core-state exchange splitting

To exemplify the role of the exchange splitting of the core states we have calculated the spectra both with and without the exchange splitting of the core states. We present here results for a model study of Fe in $Fe_{0.5}Ni_{0.5}$, because the influence on Fe is expected to be the largest of the studied materials. The computed spin splitting of the $j_z=-3/2$ and $+3/2$ sublevels is almost 1 eV for Fe in $Fe_{0.5}Ni_{0.5}$ and smaller for Co and Ni. It is instructive to consider the absorption coefficients $\alpha^{\pm}$ for left- and right-circularly polarized in the polar geometry, which are related to the refractive indices $n_{\pm}$ by $\alpha^{\pm}=2\omega\,\mathrm{Im}\,n_{\pm}/c$. In Fig. 6 we show the total absorption spectrum $\alpha^{+}+\alpha^{-}$ as well as the XMCD spectrum $\alpha^{+}-\alpha^{-}$ as obtained with or without the exchange splitting of the $2p$ core states taken into account. The inclusion of the exchange splitting of the core states modifies the

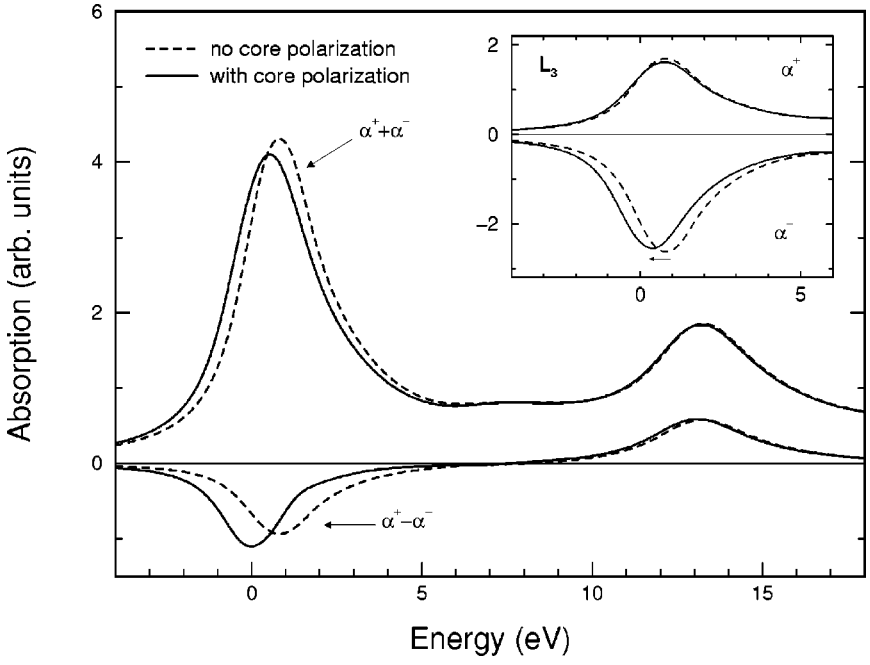

FIG. 6. Study of the influence of the spin polarization of the $2p$ core states on the absorption coefficients α^{+} and α^{-} for right- and left-circularly polarized light, respectively. The absorption coefficients are calculated for the L edge of Fe in the $Fe_{0.5}Ni_{0.5}$ alloy. The total absorption is given by $\alpha^{+}+\alpha^{-}$, the dichroic asymmetry by $\alpha^{+}-\alpha^{-}$. The inset shows an expanded view of α^{+} and α^{-} (shown with negative sign for clarity) at the L_3 edge.

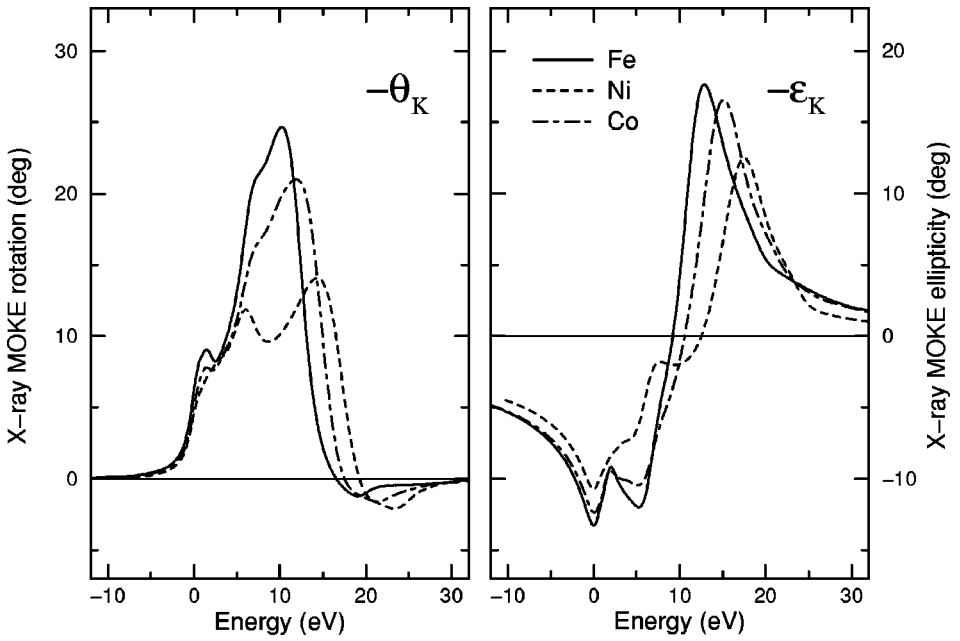

FIG. 7. *Ab initio* calculated polar x-ray MOKE rotation θ_K and ellipticity ε_K at the L edges of bcc Fe, hcp Co, and fcc Ni. The spectra have been shifted relative to the energy offset of the edge and are shown with a minus sign.

theoretical XMCD spectrum in two ways: first, the spacing of the $L_{2,3}$ peaks is increased by approximately 1 eV, and second, the slope of the low-energy side of the L_3 peak is increased, which results in a more pronounced asymmetry of the shapes of the L_2 and L_3 peaks. Both features improve the agreement with the experimental data (see Fig. 3). We further note that from a comparison of the spectra computed without core polarization and experiment, one could draw the wrong conclusion that the spin-orbit splitting of the $2p$ core state is too small, where it is actually the core-state exchange splitting that is responsible.

In order to understand in more detail the role of the exchange splitting of the core states we show the L_3 absorption coefficients for the two circular polarizations in the inset of Fig. 6 (for clarity's sake the absorption coefficient α^- is shown with a minus sign). The behavior of the absorption coefficients when the exchange splitting of the core states is ''switched on'' can be understood by considering the weights with which the transitions from the individual core states contribute to the absorption spectra. These weights are determined by the angular parts of the dipolar matrix elements, which increase with increasing j_z for negative helicity and decrease for positive helicity, and by the occupation of the final *d* states, which favors transitions to unoccupied minority ($\downarrow$) spin states. The major contribution to the α_- peak stems from the $j_z=-3/2$ level, which eigenenergy is increased by the exchange interaction. This leads to the shift of the absorption peak towards lower energies. The major contribution to the α^+ peak comes with approximately equal weight from the $j_z=-1/2$ and 1/2 sublevels. Since the exchange interaction increases and decreases, respectively, the eigenenergies of these states by the same amount, it mainly leads to a broadening of the absorption peak without shifting its center of gravity. At the L_2 the influence of the spin splitting of the $2p_{1/2}$ states is much smaller, but it can qualitatively be discussed in the same manner. Thus, although the spin splitting of the $2p$ core states is small, it nevertheless leads to an improvement of the theoretical spectra. The influence of the spin splitting of the core states was previously computed for the $L_{2,3}$ edge of Co in CoPt alloys,[23] for which similar modifications were found, but no details of their origin were given.

D. X-ray polar MOKE

Although so far no x-ray polar MOKE spectra have been measured, for the aim of comparing with future experiments we have computed these. To this end, we have employed the exact expression (8) for the magneto-x-ray rotation θ_K and ellipticity ε_K. It is, however, for the analysis of the computed x-ray MOKE spectra convenient to note that the exact expression can be approximated by[31]

$$\theta_K + i\varepsilon_K \approx i\frac{n_+ - n_-}{n_+ n_- - 1} \approx \frac{-\epsilon_{xy}}{\epsilon_{xx}^{1/2}(1-\epsilon_{xx})}. \tag{12}$$

The calculated polar MOKE spectra of bcc Fe, hcp Co, and fcc Ni are shown in Fig. 7. Unlike in the visible range where the shape of the MOKE spectra in most cases reflects the shape of the off-diagonal conductivity spectrum,[44] for the x-ray regime the denominator in Eq. (12) is found to play a crucial role. Contrary to the x-ray Faraday spectrum, the x-ray MOKE spectrum displays a large maximum *in between* the two absorption edges. A closer look at Eqs. (3) and (12) clarifies the origin of this spectral difference. Both the Faraday and polar Kerr effects contain as numerators $n_+ - n_-$, but the Kerr effect is additionally modified by the denominator $n_+ n_- - 1$. Since in the soft-x-ray range n is close to 1, a profound influence of the denominator can be anticipated. To illustrate the influence of the denominator we show in Fig. 8 the x-ray MOKE of fcc Co, as well as the separate spectra of ε_{xy} and $[1-\varepsilon_{xx}]^{-1}$. The x-ray MOKE quantities are approximately composed of the product of the latter two spectra, where $1-\varepsilon_{xx}$ is the dominating part of $\varepsilon_{xx}^{1/2}(1$

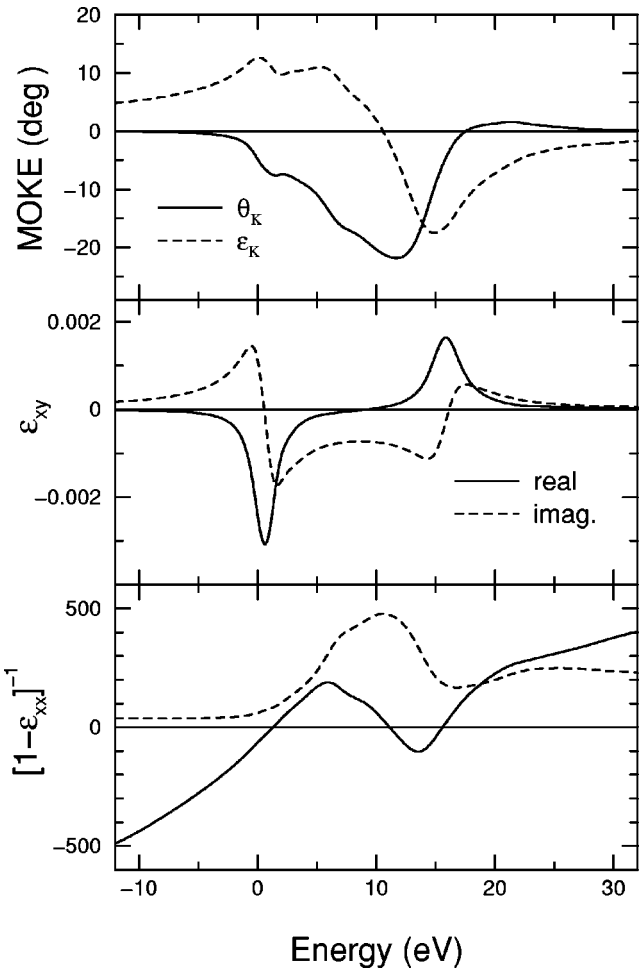

FIG. 8. Analysis of the x-ray polar MOKE spectrum at the L edge of fcc Co. In the top panel the real (i.e., θ_K) and imaginary (ε_K) part of the complex Kerr response are depicted. The middle panel shows the real and imaginary parts of ε_{xy}, which is the numerator of Eq. (12). The bottom panel shows the real and imaginary parts of the inverse of $[1-\varepsilon_{xx}]$, which is the dominating term in the denominator of Eq. (12). The product of the quantities in the middle and bottom panels leads to the x-ray Kerr rotation and ellipticity depicted in the top panel.

$-\varepsilon_{xx}$). The denominator affects the x-ray Kerr rotation such that a broad maximum occurs between the L_2 and L_3 edges, which is caused by the peak in the imaginary part of its inverse (see Fig. 8). The marked impact of the denominator implies a high sensitivity of polar MOKE measurements to surface oxidation effects. Already a surface layer would change the denominator to $n_+ n_- - n_s^2$, where n_s is the refractive index of the surface layer.[31]

E. Spin and orbital moments

From the above-reported dichroic spectra it is evident that the experimental spectra can be very well described by the *ab initio* calculations. It has become customary in magneto-x-ray experiments to exploit the measured dichroic spectra to extract the spin and orbital moment of an element, using the sum rules.[12,13] From the computed dichroic spectra we can, using the orbital moment sum rule, now compute the orbital moment, which we can compare to the exactly computed orbital moment.[45] The question is how well these two compare. In Table I we give the exactly calculated orbital moments as well as those obtained from the theoretical spectra employing the orbital moment sum rule. There exists reasonably good agreement between the orbital moments obtained by the two different approaches. Note that in all cases the orbital moment sum rule leads to an orbital moment *smaller* than the straightforwardly calculated one. A similar result has been found too in a previous computational study.[23] Although the agreement appears reasonable, it should be mentioned that considerable uncertainties enter the evaluation of the orbital moment sum rule. First, the number of holes is not clearly defined for solids, which becomes critical in the case of almost filled final states. Second, there exists the energy cutoff for the integration (or subtraction of the background) that has to be fixed in the integration of the total absorption. This procedure is arbitrary even in the theoretical calculation, since the accessible final states of d symmetry originate not only from the considered atom (in a tight-binding sense). This difficulty is easily demonstrated by integrating the d partial density of states up to high energies (more than 40 eV above the Fermi energy) yielding a number of d states larger than 10. On account of this difficulty, an uncertainty in the determination of the orbital moments from the sum rule can be estimated to be 10%-20% for the here-considered materials. Such uncertainty would appear to limit an accurate determination of orbital moments from measured dichroic spectra with the sum rule. Considering, however, the fact that the sum rules are derived only for isolated atoms[12,13] and involve a large number of approximations,[23] it is remarkable how reasonable the obtained orbital moments nevertheless are. Larger deviations (up to 50%) were previously obtained in a theoretical investigation of the sum rule for the spin moment.[46] To end with, we remark that recently an exact sum rule for the orbital moment of solids has been reported by two of us,[47] which, however, requires an integration over an unrestricted magneto-optical spectrum.

TABLE I. The orbital moments obtained for various ferromagnetic $3d$ materials. The exactly calculated orbital moment is denoted by M_l (calc.), whereas M_l (s rule) denotes the orbital moment derived from the sum rule. M_s is the computed spin moment and n_d the calculated number of holes in the $3d$ band.

	M_l (calc.)	M_l (s rule)	n_d	M_s
Fe (FeNi)	0.072	0.067	6.04	2.76
Ni (FeNi)	0.056	0.052	8.26	0.71
bcc Fe	0.047	0.041	6.04	2.23
fcc Ni	0.052	0.043	8.18	0.62
fcc Co	0.075	0.070	7.20	1.64
hcp Co	0.081	0.074	7.24	1.63

VI. CONCLUSIONS

We have carried out *ab initio* calculations and experiments of the x-ray Faraday effect at the $L_{2,3}$ edges of Fe, Co,

and Ni. Our investigations demonstrate that the measured and calculated dichroic spectra at the L edges of the $3d$ ferromagnets are in good agreement. Since the theory of x-ray magneto-optical effects can be formulated in terms of components of the dielectric tensor, we can anticipate that also other x-ray magneto-optical effects as the x-ray MOKE can be explained by first-principles theory. For comparison with future experiments we have computed the polar x-ray MOKE of Fe, Co, and Ni.

Our *ab initio* calculations show explicitly that the many-particle x-ray excitation spectrum can to a good approximation be replaced by the single-particle Kohn-Sham spectrum. The good agreement between the calculated and experimental x-ray magneto-optical spectra suggests that for the investigated materials the role of many-particle contributions to the excitation spectra, such as, e.g., core-hole effects, is limited to a possible renormalization of the edge transition energy, without any major impact upon the shape of the spectra. An exception could be the weak shoulder in the $\Delta\beta$ spectrum at the L_3 edge of Ni, which deserved further study. Apart from this weak feature, on the basis of the present investigation we foresee no direct demand to invoke supplemental Coulomb correlation terms U for calculations of XFE, x-ray MOKE, or XMCD spectra. The need for Coulomb correlation effects has previously been argued for the explanation of photoemission spectra obtained from the $2p$ states. We furthermore find no direct evidence that multiplet transitions are required to explain the magneto-x-ray spectra, at least not at the spectral resolutions $E/\Delta E = 2500$ and 700 used here. It could be, however, that signatures of multiplet transitions become visible at higher resolutions. Also, it might well be that multiplet excitations must be taken into account to describe the magneto-x-ray spectra of, e.g., $4f$ materials.

Our calculations reveal the influence of the exchange splitting of the core states on the dichroic spectra. Its influence is small, yet the computed dichroic spectra are improved compared to experiment when the core polarization is accounted for.

ACKNOWLEDGMENTS

This work was supported financially by the Sonderforschungsbereich 463, Dresden, Germany, and by the European Community under Project No. ERB FMG ECT 980105.

*Permanent address: Institute of Physics, Academy of Sciences, Cukrovarnická 10, CZ-162 53 Prague, Czech Republic.

[1] G. van der Laan, B.T. Thole, G.A. Sawatzky, J.B. Goedkoop, J.C. Fuggle, J.M. Esteva, R.C. Karnatak, J.P. Remeika, and H.A. Dabkowska, Phys. Rev. B **34**, 6529 (1986).

[2] G. Schütz, W. Wagner, W. Wilhelm, P. Kienle, R. Zeller, R. Frahm, and G. Materlik, Phys. Rev. Lett. **58**, 737 (1987).

[3] D. Gibbs, D.R. Harshman, E.D. Isaacs, D.B. McWhan, D. Mills, and C. Vettier, Phys. Rev. Lett. **61**, 1241 (1988).

[4] D.P. Siddons, M. Hart, Y. Amemiya, and J.B. Hastings, Phys. Rev. Lett. **64**, 1967 (1990).

[5] C.C. Kao, J.B. Hastings, E.D. Johnson, D.P. Siddons, G.C. Smith, and G.A. Prinz, Phys. Rev. Lett. **65**, 373 (1990).

[6] J.B. Kortright, M. Rice, and R. Carr, Phys. Rev. B **51**, 10 240 (1995).

[7] J.B. Kortright, M. Rice, S.-K. Kim, C.C. Walton, and T. Warwick, J. Magn. Magn. Mater. **191**, 79 (1999).

[8] S.P. Collins, J. Phys.: Condens. Matter **11**, 1159 (1999).

[9] H.-Ch. Mertins, F. Schäfers, X. Le Cann, A. Gaupp, and W. Gudat, Phys. Rev. B **61**, R874 (2000).

[10] H.-Ch. Mertins, F. Schäfers, A. Gaupp, W. Gudat, J. Kuneš, and P. M. Oppeneer, Nucl. Instrum. Methods Phys. Res. A **467&468**, 1407 (2001).

[11] H.-Ch. Mertins, F. Schäfers, and A. Gaupp, Europhys. Lett. **55**, 125 (2001).

[12] B.T. Thole, P. Carra, F. Sette, and G. van der Laan, Phys. Rev. Lett. **68**, 1943 (1992).

[13] P. Carra, B.T. Thole, M. Altarelli, and X. Wang, Phys. Rev. Lett. **70**, 694 (1993).

[14] C.T. Chen, Y.U. Idzerda, H.-J. Lin, N.V. Smith, G. Meigs, E. Chaban, G.H. Ho, E. Pellegrin, and F. Sette, Phys. Rev. Lett. **75**, 152 (1995).

[15] D. Weller, J. Stöhr, R. Nakajima, A. Carl, M.G. Samant, C. Chappert, R. Mégy, P. Beauvillain, P. Veillet, and G.A. Held, Phys. Rev. Lett. **75**, 3752 (1995).

[16] D. Arvanitis, M. Tischer, J. Hunter Dunn, F. May, N. Mårtensson, and K. Baberschke, in *Spin-Orbit-Influenced Spectroscopies of Magnetic Solids*, edited by H. Ebert and G. Schütz (Springer, Berlin, 1996), p. 145.

[17] N. Nakajima, T. Koide, T. Shidara, H. Miyauchi, H. Fukutani, A. Fujimori, K. Iio, T. Katayama, M. Nývlt, and Y. Suzuki, Phys. Rev. Lett. **81**, 5229 (1998).

[18] P. Kuiper, B.G. Searle, P. Rudolf, L.H. Tjeng, and C.T. Chen, Phys. Rev. Lett. **70**, 1549 (1993).

[19] M.M. Schwickert, G.Y. Guo, M.A. Tomaz, W.L. O'Brien, and G.R. Harp, Phys. Rev. B **58**, R4289 (1998).

[20] J. Igarashi and K. Hirai, Phys. Rev. B **50**, 17 820 (1994).

[21] H.J. Gotsis and P. Strange, J. Magn. Magn. Mater. **140–144**, 2171 (1995).

[22] N. Mainkar, D.A. Browne, and J. Callaway, Phys. Rev. B **53**, 3692 (1996).

[23] H. Ebert, in *Spin-Orbit-Influenced Spectroscopies of Magnetic Solids*, edited by H. Ebert and G. Schütz (Springer, Berlin, 1996), p. 159.

[24] H.J. Gotsis and P. Strange, Phys. Rev. B **55**, 12 826 (1997).

[25] G.Y. Guo, Phys. Rev. B **55**, 11 619 (1997).

[26] A.L. Ankudinov and J.J. Rehr, Phys. Rev. B **56**, R1712 (1997).

[27] W. Kohn and L. Sham, Phys. Rev. **140**, A1133 (1965); U. von Barth and L.A. Hedin, J. Phys. C **5**, 1692 (1972).

[28] H. Petersen, M. Willmann, F. Schäfers, and W. Gudat, Nucl. Instrum. Methods Phys. Res. A **333**, 594 (1993).

[29] M. Weiss, K.J.S. Sawhney, R. Follath, H.-Ch. Mertins, F. Schäfers, A. Gaupp, J. Bahrdt, F. Senf, and W. Gudat, in *Synchrotron Radiation Instrumentation*, edited by P. Pianetta, J. Arthur, and S. Brennan, AIP Conf. Proc. No. 521 (AIP, New York, 2000), p. 134.

[30] F. Schäfers, H.-Ch. Mertins, A. Gaupp, W. Gudat, M. Mertin, I.

Packe, F. Schmolla, S. Di Fonzo, G. Soullié, W. Jark, R. Walker, X. Le Cann, M. Eriksson, and R. Nyholm, Appl. Opt. **38**, 4074 (1999).

[31] P.M. Oppeneer, Habilitation thesis, University of Technology, Dresden, 1999; in *Handbook of Magnetic Materials*, edited by K.H.J. Buschow (Elsevier, Amsterdam, 2001), Vol. 13, pp. 229-422.

[32] Note that we use here again the indices "*xy*" to denote the off-diagonal permittivity, which can be done after a simple coordinate transformation.

[33] S.W. Lovesey and S.P. Collins, *X-ray Scattering and Absorption by Magnetic Materials* (Clarendon Press, Oxford, 1996).

[34] O. Hellwig, J.B. Kortright, K. Takano, and E.E. Fullerton, Phys. Rev. B **62**, 11 694 (2000).

[35] T. Kraft, P.M. Oppeneer, V.N. Antonov, and H. Eschrig, Phys. Rev. B **52**, 3561 (1995).

[36] P. Blaha, K. Schwarz, and J. Luitz, *WIEN'97, A Full Potential Linearized Augmented Plane Wave Package for Calculating Crystal Properties* (Technical University Wien, Vienna, 1999).

[37] J. Kuneš, P. Novák, M. Diviš, and P.M. Oppeneer, Phys. Rev. B **63**, 205111 (2001).

[38] D.J. Singh, *Planewaves, Pseudopotentials and the LAPW method* (Kluwer Academic, Dordrecht, 1994).

[39] J.P. Perdew and Y. Wang, Phys. Rev. B **45**, 13 244 (1992).

[40] J.E. Muller, O. Jepsen, and J.W. Wilkins, Solid State Commun. **42**, 365 (1982).

[41] M.J. Freiser, IEEE Trans. Magn. **4**, 152 (1967).

[42] C.T. Chen, F. Sette, Y. Ma, and S. Modesti, Phys. Rev. B **42**, R7262 (1990).

[43] W.L. O'brien, B.P. Tonner, G.R. Harp, and S.S.P. Parkin, J. Appl. Phys. **76**, 6462 (1994).

[44] P.M. Oppeneer, T. Maurer, J. Sticht, and J. Kübler, Phys. Rev. B **45**, 10 924 (1992).

[45] M.S.S. Brooks and P.J. Kelly, Phys. Rev. Lett. **51**, 1708 (1983).

[46] R. Wu and A.J. Freeman, Phys. Rev. Lett. **73**, 1994 (1994).

[47] J. Kuneš and P.M. Oppeneer, Phys. Rev. B **61**, 15 774 (2000).